R-13-50

Electron irradiation accelerated Cu-precipitation experiment

Testing of canister insert cast iron and an FeCu model alloy

Pär Olsson, Zhongwen Chang
KTH Royal Institute of Technology, Reactor physics

Amine Yousfi, Mattias Thuvander
Chalmers University of Technology, Applied Physics

Bruno Boizot, Gauthier Brysbaert, Vincent Metayer,
Dominique Gorse-Pomonti
CNRS-LSI, Ecole Polytechnique

December 2013

Svensk Kärnbränslehantering AB
Swedish Nuclear Fuel
and Waste Management Co

Box 250, SE-101 24 Stockholm
Phone +46 8 459 84 00

ISSN 1402-3091
SKB R-13-50
ID 1417835

Electron irradiation accelerated Cu-precipitation experiment

Testing of canister insert cast iron and an FeCu model alloy

Pär Olsson, Zhongwen Chang
KTH Royal Institute of Technology, Reactor physics

Amine Yousfi, Mattias Thuvander
Chalmers University of Technology, Applied Physics

Bruno Boizot, Gauthier Brysbaert, Vincent Metayer,
Dominique Gorse-Pomonti
CNRS-LSI, Ecole Polytechnique

December 2013

Summary

Cast iron and FeCu model alloy samples were electron irradiated during one week in order to accelerate the ageing process to replicate the conditions for the cast iron insert in the repository for spent nuclear fuel in Sweden. The goal of the study was to determine if there could be copper precipitation in the cast iron as an effect of the gamma irradiation conditions. Copper precipitation causes hardening and may cause embrittlement in certain conditions. A rate theory model was used in order to calculate the acceleration factor of the ageing processes in the samples. The acceleration factor was estimated to 2,750, meaning that one week of electron irradiation corresponds to 45 years in storage conditions. For the cast iron samples it is non-trivial to provide a good correction to the acceleration factor due to the effect of the graphite nodules without further studies. During the irradiation, the room temperature resistivity of the samples was measured but no conclusions could be drawn due to large data scatter. After the irradiation campaign, the samples were analyzed using atom probe tomography. There, it was clearly seen that in the FeCu model alloy, copper starts to precipitate, while in the cast iron samples no precipitation was seen.

Sammanfattning

Gjutjärn- och FeCu-modellegeringsprov elektronbestrålades under en vecka för att accelerera åldrandeprocessen som sker i gjutjärnet som ska användas i det svenska slutförvaret för använt kärnbränsle. Målet med studien var att avgöra om koppar kan fällas ut i gjutjärnet på grund av gammabestrålningen. Kopparutfällning orsakar förhärdning av materialet vilket kan leda till försprödning under vissa förhållanden. En rate-teorimodell användes för att beräkna accelerationsfaktorn för åldringsprocessen. Accelerationsfaktorn bestämdes till 2 750, vilket innebär att en veckas bestrålning motsvarar ca 45 års lagring. För gjutjärnsproven är det svårt att avgöra med hög tillförlitlighet hur accelerationsfaktorn bör korrigeras på grund av effekten av grafitnodulerna utan att genomföra vidare studier. Under bestrålningen mättes provens resistivitet vid rumstemperatur *in situ* men inga slutsatser kunde dras på grund av den stora spridningen av data. Efter bestrålningen analyserades proven med en tomografisk atomsond. Där syntes det tydligt att koppar börjar fällas ut i det bestrålade FeCu-legeringsprovet, medan ingen effekt av bestrålningen upptäcktes i gjutjärnsproven.

Contents

1 Introduction

A well-known problem in pressurized water reactors (PWR) is the hardening and embrittlement induced by precipitation of Cu particles in the vessel, which is mainly composed of α-Fe. The accelerated ageing process spans over several decades and is thus relevant for the reactor life time. Cu precipitation under irradiation or during thermal ageing has been extensively studied experimentally and theoretically since more than four decades due to its technological importance, see Vincent et al. (2008) for a recent review of the modeling of Cu precipitation. Similar ageing processes may be of relevance also in materials to be used for long-term storage of nuclear waste, see Brissoneau and Bocquet (2003) and Brissoneau et al. (2004). In the storage material, the dose-rate due to radioactivity is much lower compared to that in a reactor. However, since the canister material temperature, of about 100°C during the first few hundred years in the repository, is much lower than that in a PWR, about 300°C, the thermodynamic driving force due to Cu supersaturation will be stronger. At the same time, 100°C is not so low as to completely inhibit diffusion, which is the case for the extreme long term perspective of hundreds of thousand years, when the canister has cooled off and its temperature approaches that of the bed rock. One must also consider that the balance between defect production and defect annihilation in the storage material will be different from that in a PWR. According to Brissoneau and Bocquet (2003) and Brissoneau et al. (2004), a high concentration of small copper particles will form in the steel or cast-iron fuel holders due to gamma-radiation from spent nuclear fuel. This will lead to an increase in the yield-strength, and consequently, an increase in the ductileto-brittle transition temperature (DBTT) of roughly 50 K. This increase would occur over 20 to 100 years, and could potentially lead to room temperature embrittlement. There are no direct experiments with which the predictions of Brissoneau and Bocquet (2003) and Brissoneau et al. (2004) can be compared, so they should be regarded as an indication of a potential problem. These predictions may be of importance also for the conditions in the Swedish spent fuel repository. In the report by Sandberg and Korzhavyi (2009), the authors predict that the supersaturated Cu is completely precipitated out from the ferrite matrix in the conditions relevant for the Swedish spent fuel repository. A high density of small Cu particles form, in the range between 10–20 Å in radius, which is the interval in which the strengthening effect is largest, according to the model of Russel and Brown (1972).

For the abovementioned reasons, we have here performed an accelerated ageing experiment of the relevant materials in order to ascertain if the predictions conform to reality. The precipitation kinetics can be accelerated by several means, whereof the two most efficient and straightforward would be temperature acceleration and irradiation acceleration. Both these techniques have, however, non-linear effects on the time scale acceleration with respect to temperature and dose rate. Therefore, careful modeling of the same effects must be performed in order to estimate the corresponding time in the repository conditions. The acceleration is here performed using electrons, for which the conditions can be well controlled and modulated. This type of irradiation can be comparable to the gamma irradiation conditions in the spent fuel canisters as long as the electrons only produce Frenkel pairs and as long as the self-interstitial atoms do not significantly interact with the different solute atoms, both of which are the cases here.

2 Experimental

2.1 Samples

The samples were of dimensions 16×4×2 mm and were mechanically polished using fine grit paper to a bright sheen on the side facing the electron beam. Eight samples from two different sets of materials were used in the study. Six cast iron samples were taken from the same region in insert I53 from SKB. As a reference material, two samples of a model FeCu alloy from the REVE project, see Jumel et al. (2002), were obtained. The nominal compositions of the cast iron and the FeCu alloy are shown in Table 2-1. The copper content of the reference alloy is higher than that of the cast iron, and thus the results may be difficult to compare directly. The very large differences in carbon and silicon compositions must also be noted, although in the cast iron, the majority of the carbon is present in graphite nodules.

Three cast iron samples and one reference alloy sample were mounted in the beam line. Thin copper wires were point soldered to the ends of the sample bars for resistivity measurements.

2.2 Electron irradiation

The samples were irradiated at the Irradiated Solids Laboratory (LSI) in Palaiseau, France, using the SIRIUS electron irradiation facility which is a high energy electron Pelletron accelerator from NEC. The current was set to 20 μA at a kinetic energy of 2 MeV. This electron beam current was sufficient in order to obtain a rather stable irradiation temperature of 140°C. Coupled with the sample geometry and the damage cross section, this gave rise to a damage flux of 1.2×10^{-8} dpa/s (displacements per atom/s). The irradiation was conducted over a period of seven days, with a few pauses to perform resistivity measurements as well as a few un-planned beam trips. A total irradiation time of 143 hours was obtained for a total damage dose of 6.7×10^{-3} dpa. The range of 2 MeV electrons in iron is about 1.7 mm according to Ishino et al. (2003). The experiment beam line setup is displayed in Figure 2-1.

2.3 Resistivity measurement

The electrical resistivity of a material is strongly dependent on its microstructure. Solute atoms, point defects and complex defects all carry residual resistivities that increase the global resistivity of a sample. During electron irradiation, the resistivity of a sample is increased due to the generation of point defects. In isochronal annealing experiments where the resistivity recovery is studied, self-interstitials in Fe are mobile from 120 K and vacancies from about 250 K (Takaki et al. 1983). Considering the high mobility of the point defects at and above room temperature, once the electron beam is switched off, the resistivity should return to its nominal value rapidly since most of the defects recombine, unless solute atoms that carry residual resistivity have been depleted from the matrix and formed precipitates. The residual resistivity of solute Cu in ferrite has been estimated to 0.25×10^{-8} Ωm/at.%Cu, according to as yet unpublished work by Chimi.

Table 2-1. Nominal compositions of the materials used in the irradiation experiment.

Element (at. %)	Cast iron	FeCu alloy
Cu	0.028	0.079
Mn	0.141	0.010
Ni	0.329	< 0.005
C	14.6	< 0.01
P	0.039	0.011
Si	3.96	0.01
Fe	Bal.	Bal.

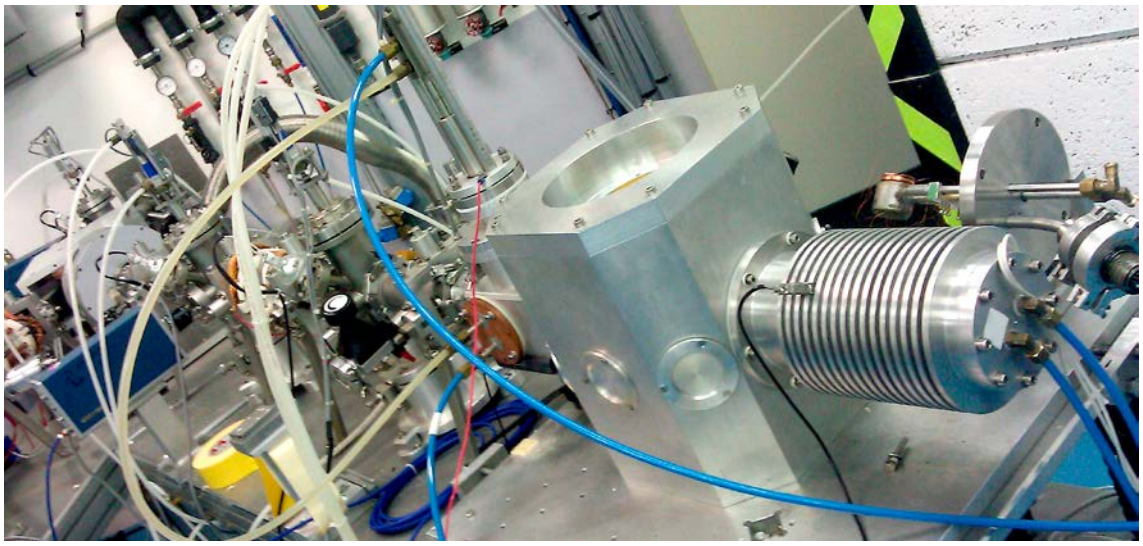

Figure 2-1. *The experimental irradiation setup. The beam line exits the wall to the far left. The octagonal chamber contains the samples. The line terminates with a beam dump. The detached sample holder, see Figure 2-2, can be seen next to the beam dump.*

A driver current of 10 mA (using a Keithley 220) was passed through the samples in order to determine the resistivity. The voltage passing through the sample at this driver current was collected with a Keithley 182 nanovoltmeter at a frequency of 1 Hz. During irradiation, the measured voltage varied too much due to the electron beam interference to be useful. The sample was irradiated and heated by the electron beam and after a few hours the beam was stopped and the sample was water cooled down to about 18°C, all the while measuring the voltage. Unfortunately, there was no water temperature regulation and there were significant fluctuations in the water temperature during the experiment. Thus the stable cool voltage was not a reasonable reference point. Instead, the 20°C voltage was used to calculate the resistivity in order to be able to compare also with the room temperature resistivity from literature. Figure 2-2 displays the sample holder with the water cooling and the resistivity measurement wires attached.

The data collection for sample 2 of cast iron was not entirely reliable, most probably due to a defective point soldered contact of the copper wires and therefore in the following we only present the data from cast iron samples 1 and 3 and from the model alloy. Due to the time constraints of the experimental campaign, we decided to gather as much data as possible for samples 1 and 3, which behaved as expected, and to maximize the total damage dose instead of attempting to fix the contact for sample 2.

The resistivity is determined from the measured voltage, applied current and the sample geometry, according to

$$\rho = \frac{RA}{L} = \frac{VA}{IL} \qquad \text{(Equation 2-1)}$$

where R is the resistance, A is the cross section area, L is the length, V is the voltage and I is the current. The samples used here were unfortunately not optimal for resistivity measurements, since they should be as close to one-dimensional as is practical.

2.4 Atom probe tomography

The irradiated test pieces were first ground gently on the side facing the electron beam and then they were ground from the other side until the thickness was about 0.3 mm. In this way the final sample will be around 0.15 mm below the irradiated surface. The non-irradiated materials were prepared in the same way. Atom probe tomography (APT) samples of the FeCu-model material were made using the standard two-stage electropolishing method. It was also attempted to use the same method for the cast iron material, but without success. Considering the average size of the graphite nodules, of about 0.1 mm, this is to be expected. For the cast iron, it is therefore necessary to use focused ion beam milling, also a non-trivial task for such an inhomogeneous material.

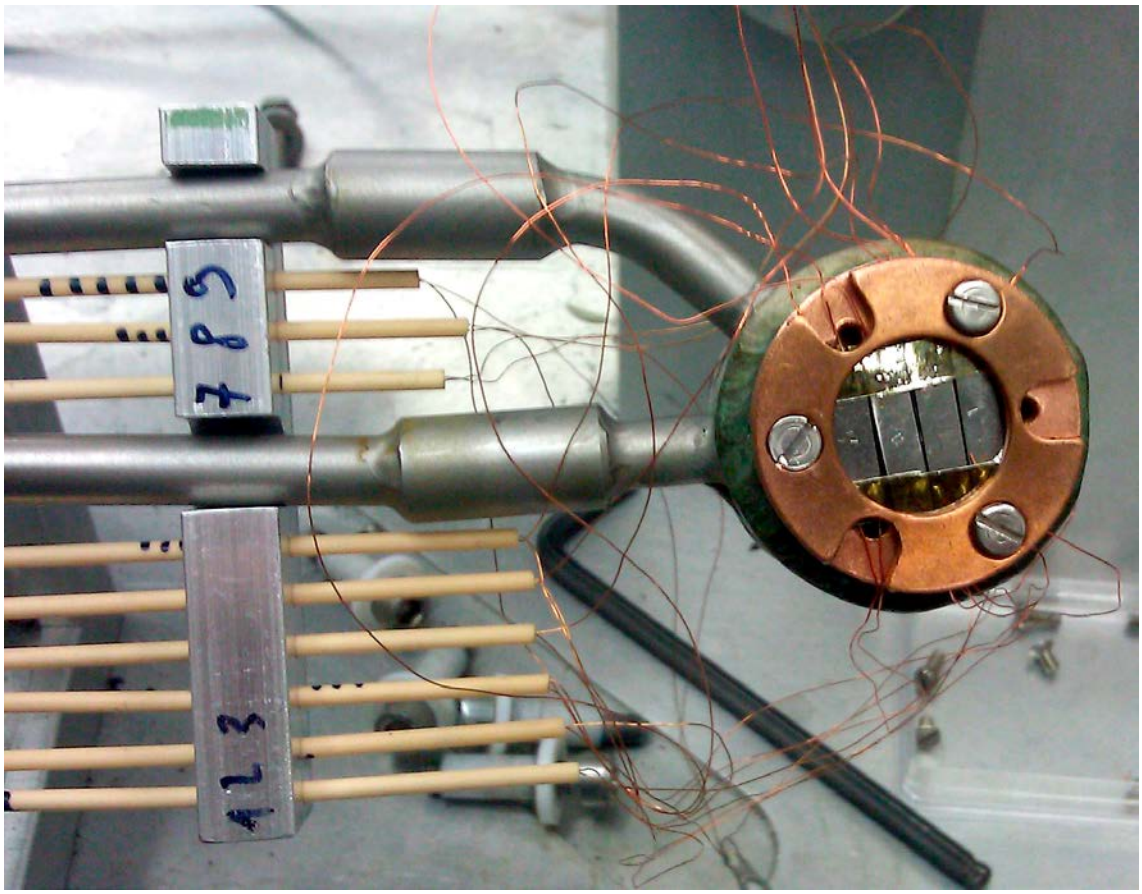

Figure 2-2. *The sample holder with the water cooling pipes, the insulated copper wires for the resistivity measurement and the four samples, separated by a thin insulator. The diameter of the electron beam is slightly greater than that of the copper holder ring.*

The materials were analyzed using a wide-angle local electrode atom probe (Imago LEAP 3000X HR) equipped with a reflectron for improved mass resolution. The analyses were carried out in voltage pulse mode with a pulse fraction of 20% and a pulse frequency of 200 kHz. The sample temperature was 70 K, and the DC voltage was regulated to keep an evaporation rate of 0.5% (ions/pulse).

The APT data was evaluated using the software IVAS 3.4/3.6. The reconstructions were made using the voltage method, with an evaporation field of 33 V/nm and a field factor of 3.8. In addition to atom maps, the statistical tools radial distribution function (RDF), nearest neighbor distance distribution (NNDD) and a clustering algorithm were applied to study the distribution of copper. The RDF is constructed as the average of radial concentration profiles centered on each Cu atom. If there is clustering, the concentration (or the relative concentration) will be high at very short distances. This is a very sensitive method to detect clustering, see for example Thuvander et al. (2012). The NNDD plots the distribution of distances between Cu-Cu nearest neighbors (the distance between two Cu atoms), and the result is compared with the same distribution calculated from a randomized dataset (with the same atom positions as in the experimental dataset, but with the atom identities exchanged at random). In case the experimental NNDD is shifted towards shorter distances, compared with the randomized NNDD, there is a tendency of clustering. The cluster algorithm used is incorporated in the IVAS software, and it has emerged as the standard algorithm for clustering studies. However, it should be noted that as there is no strict definition of clusters, the choice of parameters in the algorithm is somewhat arbitrary. In the present study the following parameter were chosen; d_{max}=1.2 nm and N_{min}=5. For further information on the cluster algorithm, see Cerezo and Davin (2005).

3 Computational model

In order to determine how long time in repository conditions an electron irradiation corresponds to, one can build a model for the evolution of the microstructure. In the report by Sandberg and Korzhavyi (2009), a rate theory model was constructed in the spirit of Brissonneau et al. (2004). The results in the Sandberg and Korzhavyi report compared well with those obtained with the older treatment and in this report we use the same methodology as Sandberg and Korzhavyi.

The defect flux in the spent fuel canister is considered to be that of the G4-fuel used in the study of Brissonneau et al. (2004). This defect flux is there stated to be in close accordance with that calculated by Guinan (2001) for the Swedish repository. We choose to use the G4-flux for consistency with Sandberg and Korzhavyi (2009). It should be noted that the G4-flux thus calculated starts from when the fuel is taken from the reactor and consequently overestimates the damage. The defect flux due to the gamma radiation rate from Brissonneau et al. (2004) is

$$g = ae^{xt} + be^{yt} + f \qquad \text{(Equation 3-1)}$$

where $a = 2.27\times10^{-15}$ dpa/s, $x = -2.85\times10^{-8}$ s^{-1}, $b = 1.8\times10^{-16}$ dpa/s, $y = -7.4\times10^{-10}$ s^{-1} and $f = 2\times10^{-20}$ dpa/s. The first term, describing the rapid decay chains, will vanish before the fuel is put in the repository canisters. The best measure of determining the time progression, while comparing different irradiation and thermal conditions, is in this study the integrated copper diffusion (ICD)

$$\text{ICD} = \int_0^t D_{Cu}(t)dt = \frac{c_v}{c_v^{th}} \int_0^t D_{Cu}^{th}(t)dt, \qquad \text{(Equation 3-2)}$$

where c_v is the actual concentration of vacancies, c_v^{th} is the thermal equilibrium concentration of vacancies and D_{Cu}^{th} is the thermal equilibrium Cu diffusion coefficient and D_{Cu} is the copper diffusivity. The rate theory model depends strongly on the parameter set used as input. Notably for Fe and dilute Fe alloys, in the literature two different sets of vacancy formation and migration energies are used, see Table 3-1. These two datasets correspond to the conditions for vacancy diffusion in low- and high-carbon containing Fe alloys, respectively. The strong vacancy-carbon binding changes the average vacancy migration in high-C alloys. Note that the Fe self-diffusion is largely unchanged by the choice of parameter set, according to Sandberg and Korzhavyi (2009), since the activation energies are almost identical. In this study we have used the high-C parameters.

Using this parameter set and the model of Sandberg and Korzhavyi (2009), 300 years of gamma irradiation at 100°C corresponds to an integrated copper diffusion of about 4.8×10^{-12} cm^2, see Figure 3-1.

In order to determine the corresponding time from the accelerated experiment, the temperature of 140°C and the damage rate due to the electron irradiation flux of 1.2×10^{-8} dpa/s was used in the same rate theory model. The ICD can then be matched between the two simulated experiments. The 143 hours of electron irradiation corresponds, according to the rate theory model, to an ICD of about 1.2×10^{-12} cm^2. Matching that ICD to the G4-flux conditions, see Figure 3-1, we estimate that the actual electron irradiation experiment corresponds to about 45 years in G4-flux conditions. This estimate is conservative when the repository conditions are considered, since the first term of Equation 3-1 will vanish during the intermediate storage phase of 15–30 years. Note that while this acceleration factor is quite reasonable for the relatively pure FeCu alloy, it is not as reliable for the cast iron due to the unaccounted effect of graphite nodules acting as sinks for defects. In the presently used rate theory model, the only considered sinks are dislocations. If graphite nodules can attract point defects to a significant extent, then this can bias the results slightly. However, the dislocations will be the dominating sinks since their density is much higher than that of the graphite nodules. The time acceleration may thus be slightly smaller for the cast iron samples. A more detailed study, including analysis of the nodule volume fraction and interfacial area, would be necessary in order to evaluate this properly.

Table 3-1. The enthalpies of vacancy formation (H_v^f), vacancy migration (H_v^m) and vacancy assisted copper activation (H_{Cu}^a) for low- and high-carbon Fe alloys.

Condition	H_v^f (eV)	H_v^m (eV)	H_{Cu}^a (eV)
Low-C	2.15 [a]	0.71 [a]	2.29 [c]
High-C	1.6 [b]	1.3 [b]	2.58 [d]

[a] Olsson et al. (2007), [b] Schaefer et al. (1977), [c] Christien and Barbu (2004), [d] Rothmann et al. (1968).

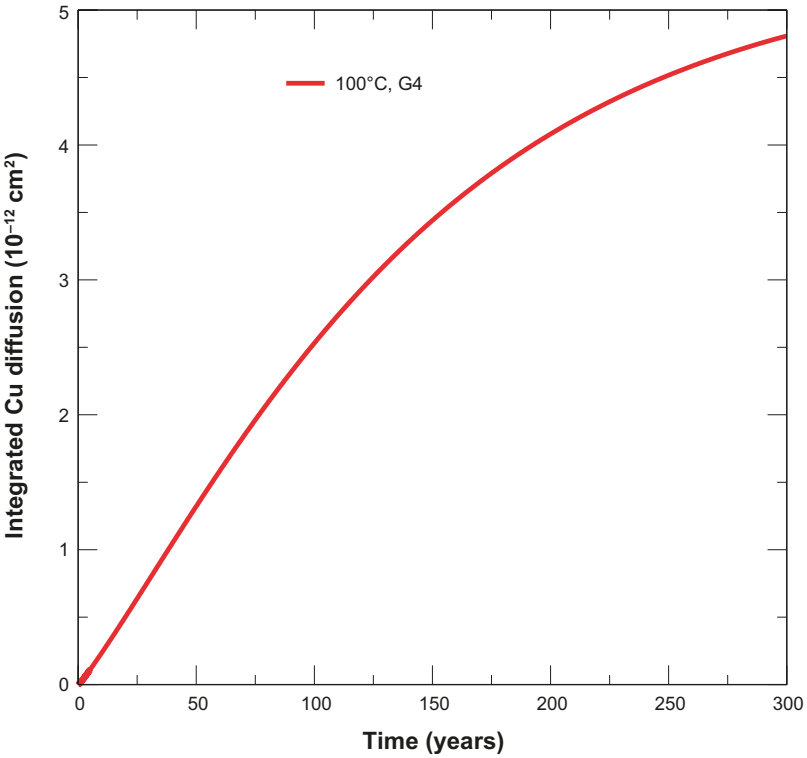

Figure 3-1. *The integrated Cu diffusion as function of time for the gamma irradiation conditions of the G4 fuel.*

4 Results

4.1 Resistivity measurements

The resistivity measurements are presented in Figure 4-1. As expected, the less pure cast iron samples have higher resistivity than the model alloy. The model alloy resistivity is reasonably close to that of pure Fe (0.97×10^{-7} Ωm (Giancoli 1995)), while the cast iron is in the high end of the range expected from malleable cast iron (~3.5×10^{-7} Ωm (Davies 1996)). The resistivity naturally increases during irradiation, due to the beam current interaction and the generation of defects in the sample. However, for the room temperature measurements, it is expected that most of the point defects will have had time to anneal out and that a change in resistivity should primarily be due to a change in the microstructure. In the case of Cu-precipitation, the resistivity should decrease as Cu is depleted from the ferrite matrix. In line with the results of Ishino et al. (2003), the expected change in resistivity, as function of dose, should be about -5×10^{-7} Ωm/dpa for the cast iron samples and -8×10^{-7} Ωm/dpa for the model alloy. The difference stems from the Cu content in the alloys, if all else is considered the same between the materials. The results of these *in situ* measurements are rather inconclusive, since the spread in resistivity for each measurement is too large to discern reliable trends in the variation. The resistivity of the cast iron samples (samples 1 and 3 in Figure 4-1) is almost constant, with a slightly positive slope for sample 3 and a slightly negative slope for sample 1. The linear regression for sample 1 almost perfectly matches the expected slope. However, these slopes cannot be considered significant considering the spread in the data. For the model FeCu alloy, there is a slightly positive slope, but the scatter is too large to draw conclusions on any Cu-precipitation. The most probable reasons for the inconclusive results are the sub-optimal sample geometry combined with a too low driver current and notably the lack of control of the water cooling temperature.

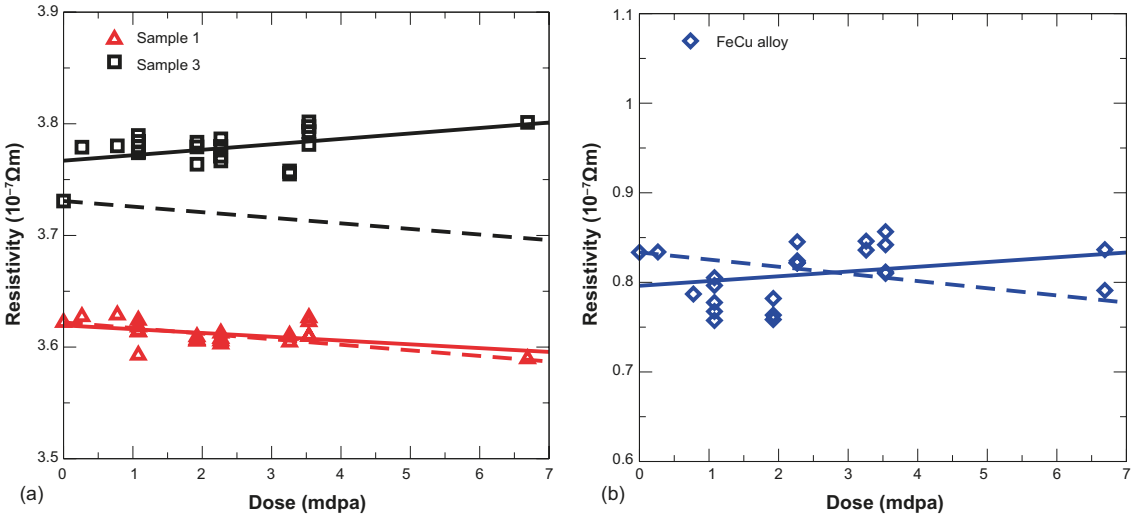

Figure 4-1. *The measured resistivity as a function of the absorbed dose during the irradiation experiment for (a) cast iron samples 1 and 3, and (b) the FeCu model alloy. The solid lines are linear regressions. The dashed lines are the expected resistivity variations considering Ishino et al. (2003). Note the difference in scale between (a) and (b).*

4.2 Atom probe tomography

The composition obtained from analysis of the irradiated and non-irradiated FeCu alloys is presented in Table 4-1. Atom maps showing the distribution of Cu for the FeCu model alloys in the entire analyzed volumes are presented in Figure 4-2. It is not easy to see any clustering in these images, but by looking at sub-volumes Cu clusters can be discerned in the irradiated material, see Figure 4-3. In order to prove that clustering has occurred in the irradiated material but not in the non-irradiated, statistical tools were applied to the datasets. In Figure 4-4 RDF curves showing the bulk-normalized concentration of Cu, measured from center Cu atoms, for the two materials are provided. The high value (approaching eight) at short distances for the irradiated material is a strong indication for clustering. The clustering is also apparent in the NNDD diagrams in Figure 4-5. Using the cluster search algorithm, the number density of clusters in the irradiated material was estimated to 6×10^{23} m^{-3}, whereas in the non-irradiated material the number density was 0.2×10^{23} m^{-3}, which essentially means that there are no clusters in the non-irradiated material. The largest cluster observed had 14 detected Cu atoms, meaning that it contained around 38 atoms (since the detection efficiency is 37%), which corresponds to a sphere of pure Cu with a radius of about 0.5 nm. This cluster size is below the resolution limit for most other microstructural analysis techniques.

Table 4-1. Composition (at.%) of FeCu-model material and cast iron sample 3 obtained from APT. Values that were not measured are denoted by *.

	Irradiated FeCu	Non-irradiated FeCu	Irradiated cast iron sample 3
Cu	0.093	0.088	0.026
Mn	0.006	0.004	0.17
Ni	*	*	0.37
Si+N	0.009	0.013	4.5
Cr	0.003	0.002	0.04
C	0.009	0.02	< 0.002
P	0.005	0.006	*
O+S	0.016	0.012	*
Fe	Bal.	Bal.	Bal.

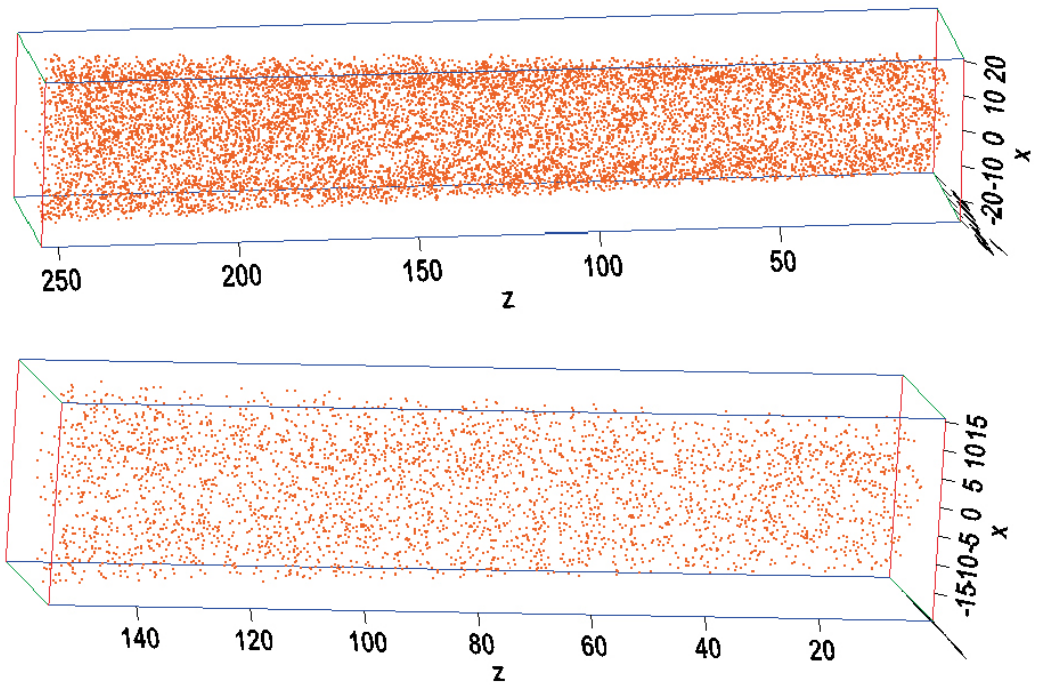

Figure 4-2. Distribution of Cu atoms in the FeCu-model alloy; irradiated (upper) and non-irradiated (lower). The reason why it appears to be a higher concentration of Cu in the upper image is that the analyzed volume is larger. The scale is in nm.

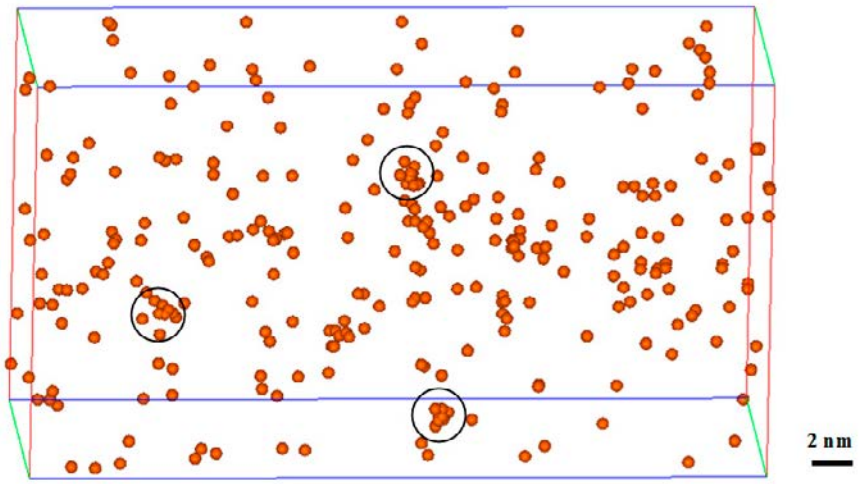

Figure 4-3. *Cu atoms in a sub-volume of the analysis of the irradiated FeCu alloy, indicating the presence of clustering. The box size is 13×19×35 nm.*

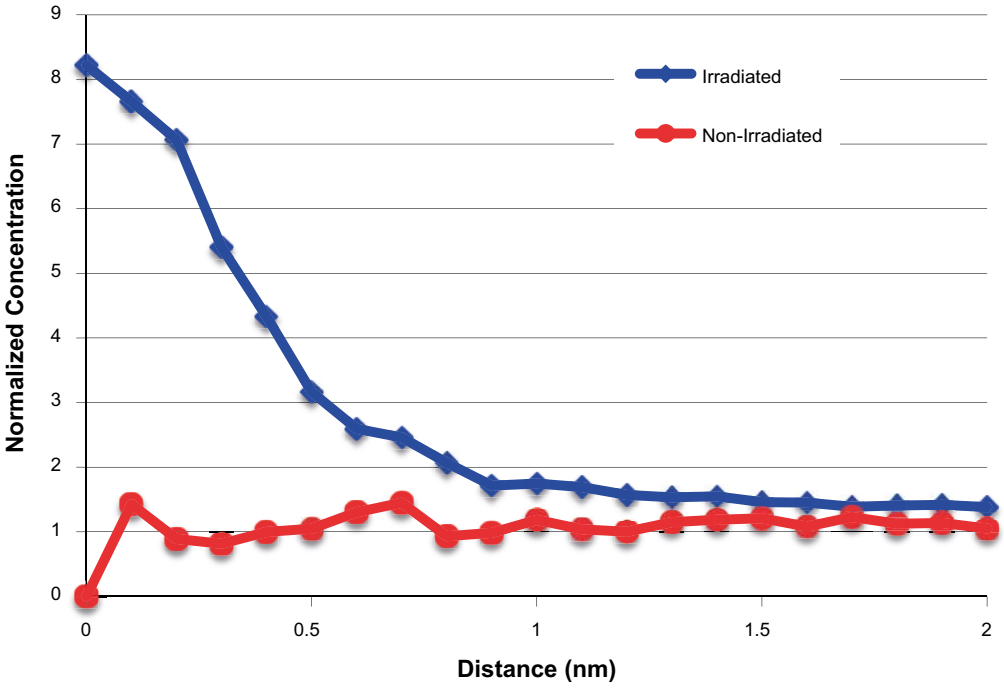

Figure 4-4. *Radial distribution function (RDF) of Cu with respect to Cu atoms for the FeCu alloy. The irradiated material shows significant clustering (strong positive interaction at short distances).*

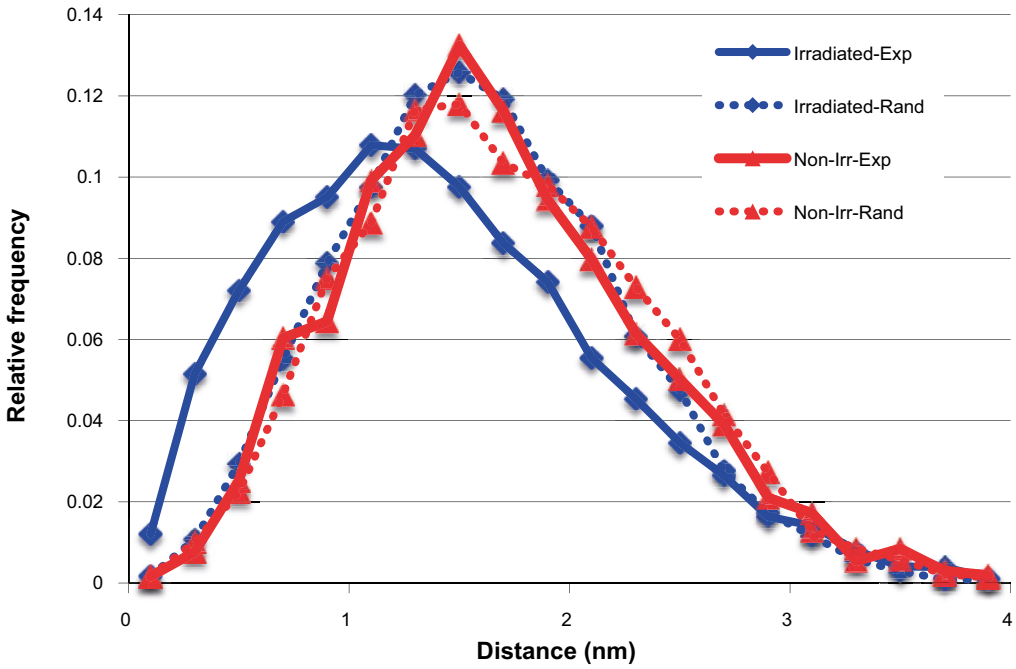

Figure 4-5. *Nearest neighbor distance distribution (NNDD) for the two FeCu-model alloy samples, together with the randomized data from each analysis. The irradiated material has much shorter distances between Cu pairs.*

For the cast iron samples, only the evaporation of a needle made from sample 3 gave sufficient statistics to be useful. There, the APT analysis showed no clustering tendencies after irradiation. The Cu-distribution and Si-distributions are displayed in Figures 4-6 and 4-7, respectively.

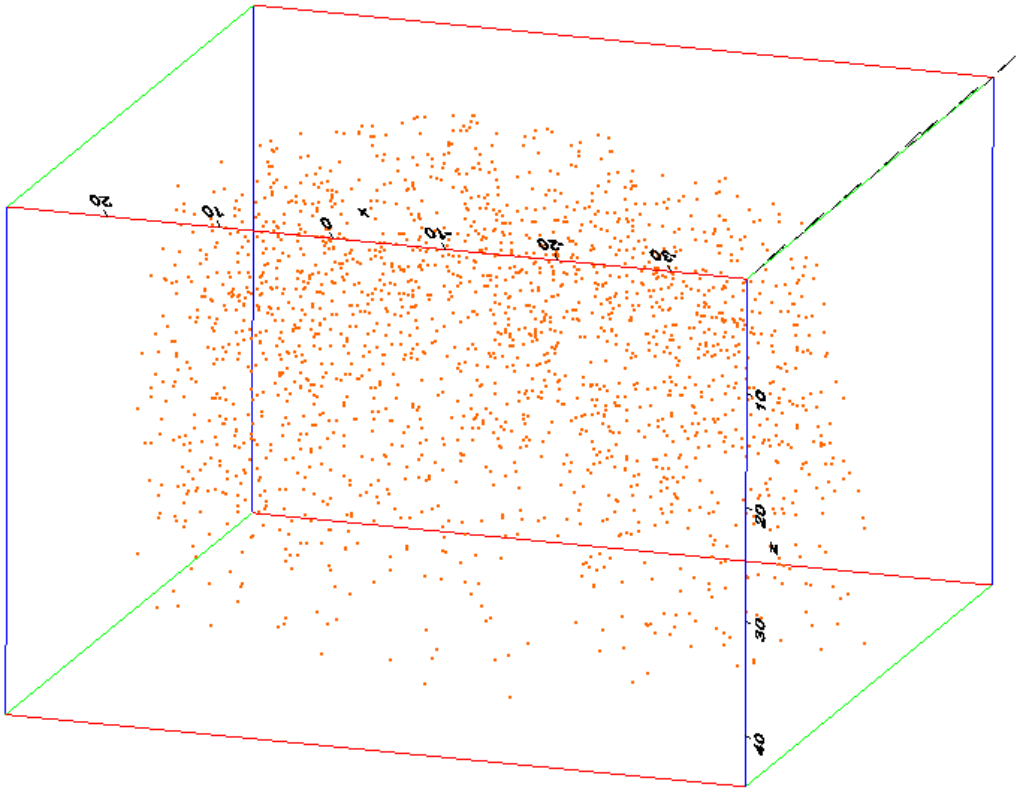

Figure 4-6. *Distribution of Cu atoms in the irradiated cast iron sample 3. The scale is in nm.*

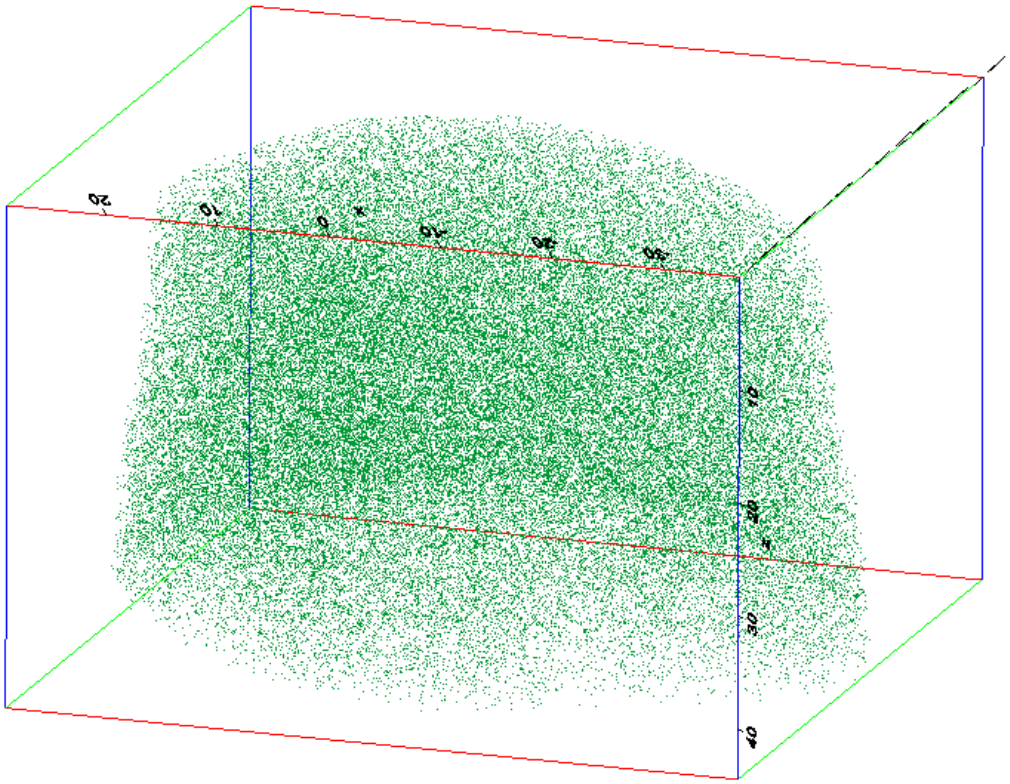

Figure 4-7. *Distribution of Si atoms in the irradiated cast iron sample 3. The scale is in nm.*

The RDF for the Cu atoms in the cast iron sample has too low statistics to be completely reliable, but as is shown in Figure 4-8, the RDF is constant, within statistical significance, around 1, implying no clustering, as can also be seen visually in Figure 4-6. The silicon content in the cast iron samples is much higher and also seems to be distributed in a fully disordered manner. The silicon distribution has a priori no influence on Cu precipitation, but shows the relative homogeneity of the studied sample. In this small atom probe specimen, almost no carbon was detected, implying that the carbon that is not in graphite nodules may be decorating e.g. dislocations or grain boundaries.

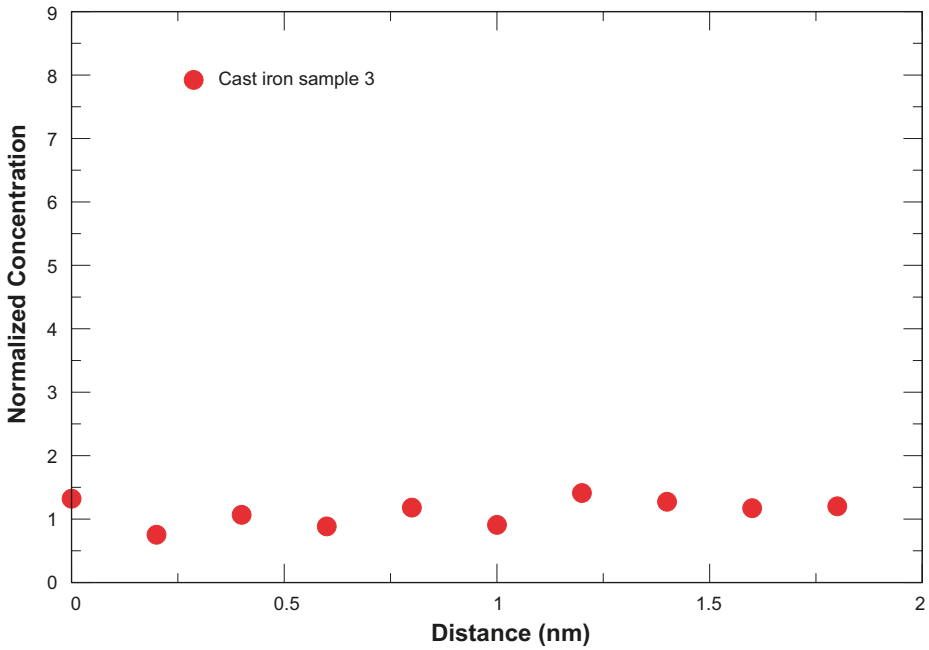

Figure 4-8. *Radial distribution function (RDF) of Cu with respect to Cu atoms for the irradiated cast iron sample 3.*

5 Conclusions

An electron irradiation experiment has been performed on cast iron and FeCu model alloy samples.

From the *in situ* resistivity measurements, no conclusions could be drawn, other than that the relative resistivities of the cast iron and model alloy samples were as expected. The sample geometry, driver current and coolant temperature control were insufficiently optimized to allow collection of reliable data.

An improved experiment setup would include *in situ* temperature regulation, to minimize temperature fluctuations, a higher driver current to increase the signal to noise ratio and an elongated wire-like sample geometry, to improve the quality of the resistivity measurement.

An overestimated damage flux function that gives a conservative effect on the copper diffusion was used in the, rate theory modeling of a highly pure FeCu alloy. It was estimated that the irradiation experiment corresponded to an acceleration of a factor of 2,750, so that the effect of gamma radiation during about 45 years at 100°C could be measured. For the cast iron samples there is a small level of uncertainty in properly determining the acceleration factor.

According to atom probe analysis, this dose was sufficient to start precipitating Cu clusters in the irradiated FeCu model alloy sample. A clear difference was seen between the un-irradiated and irradiated samples. The cluster sizes are small compared to the predictions made by Sandberg and Korzhavyi (2009) and the induced hardening should, according to the Russel-Brown model, be almost negligible after this amount of time.

In the cast iron samples, no clustering of any kind was detected with the atom probe. The absence of carbon in the analyzed volume may be due to carbon decoration on microstructure features. No hardening effects due to Cu precipitation can be expected for the cast iron inserts in the time frame to which the acceleration experiment corresponds. The length of this time, for the reasons stated above, may be slightly shorter than the 45 years that was achieved for the FeCu model alloy.

References

SKB's (Svensk Kärnbränslehantering AB) publications can be found at www.skb.se/publications.

Brissonneau L, Bocquet J-L, 2003. Radiation effects on the mechanical properties and long term aging of spent fuel storage containers. In Proceedings of 9th ASME International Conference on Radioactive Waste Management and Environmental Remediation , Vol 1. American Society Mechanical Engineers.

Brissonneau L, Barbu A, Bocquet J-L, 2004. Radiation effects on the long-term ageing of spent fuel storage containers. Packaging, Transport, Storage & Security of Radioactive Material 15, 121–130.

Cerezo A, Davin L, 2007. Aspects of the observation of clusters in the 3-dimensional atom probe. Surface and Interface Analysis 39, 184–188.

Christien F, Barbu A, 2004. Modelling of copper precipitation in iron during thermal aging and irradiation. Journal of Nuclear Materials 324, 90–96.

Davies J R (ed), 1996. Cast irons. Materials Park, OH: ASM International.

Giancoli D C, 1995. Physics: principles with applications. 4th ed. Englewood Cliffs, NJ: Prentice Hall.

Guinan M W, 2001. Radiation effects in spent nuclear fuel canisters. SKB TR-01-32, Svensk Kärnbränslehantering AB.

Ishino S, Chimi Y, Bagiyono, Tobita T, Ishikawa N, Suzuki M, Iwase A, 2003. Radiation enhanced copper clustering processes in Fe–Cu alloys during electron and ion irradiations as measured by electrical resistivity. Journal of Nuclear Materials 323, 354–359.

Jumel S, Domain C, Ruste J, Van Duysen J-C, Becquart C, Legris A, Pareige P, Barbu A, Van Walle E, Chaouadi R, Hou M, Odette G R, Stoller R E, Wirth B D, 2002. Simulation of irradiation effects in reactor pressure vessel steels: the Reactor for Virtual Experiments (REVE) project. Journal of Testing and Evaluation 30, 37–46.

Olsson P, Domain C, Wallenius J, 2007. Ab initio study of Cr interactions with point defects in bcc Fe. Physical Review B 75. doi:10.1103/PhysRevB.75.014110.

Rothman S J, Peterson N L, Walter C M, Nowicki L J, 1968. The diffusion of copper in iron. Journal of Applied Physics 39, 5041–5044.

Russell K C, Brown L M, 1972. A dispersion strengthening model based on differing elastic moduli applied to the iron–copper system. Acta Metallurgica 20, 969–974.

Sandberg N, Korzhavyi P, 2009. Theoretical study of irradiation induced hardening and embrittlement in spent nuclear fuel holders, relevant for the Swedish long-term storage. SKB R-09-15, Svensk Kärnbränslehantering AB.

Schaefer H-E, Maier K, Weller M, Herlach D, Seeger A, Diehl J, 1977. Vacancy formation in iron investigated by positron annihilation in thermal equilibrium. Scripta Metallurgica 11, 803–809.

Takaki S, Fuss J, Kuglers H, Dedek U, Schultz H, 1983. The resistivity recovery of high purity and carbon doped iron following low temperature electron irradiation. Radiation Effects 79, 87–122.

Thuvander M, Zhou J, Odqvist J, Hertzman S, Hedström P, 2012. Observations of copper clustering in a 25Cr-7Ni super duplex stainless steel during low-temperature aging under load. Philosophical Magazine Letters 92, 336–343.

Vincent E, Becquart C S, Pareige C, Pareige P, Domain C, 2008. Precipitation of the FeCu system: a critical review of atomic kinetic Monte Carlo simulations. Journal of Nuclear Materials 373, 387–401.